Why Do $Pt(PR_3)_2$ Complexes Catalyze the Alkyne Diboration Reaction, but Their Palladium Analogues Do Not? A Density Functional Study

Qiang Cui, Djamaladdin G. Musaev,* and Keiji Morokuma*

Cherry L. Emerson Center for Scientific Computation and Department of Chemistry, Emory University, Atlanta, Georgia 30322

Received April 2, 1997

The B3LYP hybrid density functional method has been applied to study theoretically the mechanism of the Pd(0)-catalyzed alkyne diboration reaction. It has been found that this reaction proceeds via the same mechanism as the Pt(0)-catalyzed diboration reaction and involves the following steps: (i) coordination of diborane R_2B-BR_2 to the Pd(0) complex, (ii) oxidative addition of the B−B bond to Pd, (iii) dissociation of one phosphine ligand, (iv) coordination of acetylene, (v) insertion of acetylene into one of the Pd−B bonds, (vi) isomerization of the resultant complex accompanied by recoordination of a phosphine ligand, and (vii) reductive elimination of the alkenyl−diboron products. However, the Pd(0) complex cannot catalyze the alkyne diboration reaction, while its Pt(0) analogue can. The main reason for this difference is found to be in the oxidative addition process of the B−B bond to $M(PH_3)_2$. This step takes place for M = Pt with a 14.0 kcal/mol activation barrier and is exothermic, but it does not take place for M = Pd, where the addition product is not stable due to a very small reverse barrier. The origin of this inactivity of Pd(0) is the $d^{10} \rightarrow sd^9$ promotion energy, which is not required for Pt(0) with the sd^9 ground state.

I. Introduction

Transition-metal-catalyzed alkene and alkyne boration reactions are attractive methods to produce the alkyl- or alkenylboron derivatives with defined regio- and stereochemistry and have increased the potential applications of boron derivatives in synthetic organic chemistry.[1] The transition-metal-catalyzed hydroboration of alkenes and alkynes with catecholborane or polyhedral boranes has been studied extensively by both experimental[1] and theoretical[2] methods. Recently, much interest has moved to Pd(0)- and Pt(0)-catalyzed alkyne and alkene diboration reactions with pinacol ester derivaties.[3] In general, it has been shown that (i) Pt(0) complexes catalyze cis addition of the B−B bond in pinacol ester derivatives, $(OCH_2)_2B-B(OCH_2)_2$, to alkynes but not to alkenes, and (ii) Pd(0) complexes, the best catalysts for the silyl- and stannylmetalation, do not catalyzed alkyne and alkene diboration reactions. The origins of the observed differences in the catalytic activity of Pt(0) and Pd(0) complexes for alkyne diboration reactions still remain unclear.

In our previous paper,[4] we reported studies of Pt(0)-catalyzed alkyne and alkene diboration reactions with $(OH)_2B-B(OH)_2$ as a model of $(OCH_2)_2B-B(OCH_2)_2$ used in the experiments.[3] In general, our findings can be summarized as follows:

(1) The Pt(0)-catalyzed alkyne/alkene diboration reaction may proceed via two different paths, A and B (see Scheme 1). Path A involves the following steps: (i) coordination of the diborane, (ii) oxidative addition of the B−B bond to the Pt(0) complex, (iii) endothermic dissociation of one of the phosphine ligands, (iv) coordination of alkyne/alkene to Pt, (v) insertion of alkyne/alkene to the Pt−B bond, (vi) isomerization of the resultant complex accompanied by recoordination of a phosphine ligand, and (vii) reductive elimination of the alkenyl/alkane−diboron products. In path B,[5] the initial step is coordination of alkyne/alkene to the Pt complex, followed by dissociation of one of the phosphine ligands and oxidative addition of the B−B bond to $Pt(PR_3)(C_2H_x)$ in either a planar (where atoms B, B, C, C, and P are on the same plane) or perpendicular (where BPtB and PPtC planes are perpendicular to each other) manner, leading to a square-planar or tetrahedral intermediate, $(BR_2)_2Pt(PR_3)(C_2H_x)$, respectively. The tetrahedral intermediate lies 4.4 kcal/mol lower than the planar cis intermediate, which is also involved in path A and is separated from the latter with a small barrier. However, the barrier from the tetrahedral to the planar trans intermediate is high (21 kcal/mol). Therefore, we conclude that the tetrahedral intermediate $(BR_2)_2Pt(PR_3)(C_2H_x)$ will rearrange to the square-planar cis intermediate and paths A and B will merge. By comparing these two paths and calculating the binding energies of $Pt(PR_3)_2$ with bulkier diboranes B_2R_2 and substituted alkynes/alkenes used in the experiments, we conclude that path A is energetically more favorable than path B in the real Pt(0)-catalyzed alkyne/alkene diboration reaction.

(2) The observed different catalytic behavior of $Pt(PH_3)_2$ on the two substrates, C_2H_2 (reactive) and C_2H_4 (nonreactive), is the result of the differences in the barrier heights for insertion of hydrocarbons into the Pt−B bond, which is calculated to be 9.0 and 22.9 kcal/mol for C_2H_2 and C_2H_4, respectively. This difference is essentially dictated by the thermochemistry of the

S0276-7333(97)00277-X CCC: $15.00
Publication on Web 01/30/1998

insertion process, $Pt(PH_3)[BR_2]_2(C_2H_X) \rightarrow Pt(PH_3)(BR_2\text{-}C_2H_xBR_2)$, which is found to be 28.1 kcal/mol exothermic for C_2H_2, but 4.1 kcal/mol endothermic for C_2H_4, and has been explained in terms of a smaller substrate deformation energy and a larger B−C "bond" energy in $Pt(PH_3)(BR_2C_2H_xBR_2)$ for C_2H_2 than for C_2H_4.

The present work is a continuation of our previous studies,[4,5] and the goal is to investigate the mechanism of the alkyne diboration reaction with the Pd(0) complex at the same level of theory. We believe that, by comparing the mechanism of the reaction

$$M(PH_3)_2 + C_2H_2 + R_2B{-}BR_2 \rightarrow M(PH_3)_2 + (HR_2B)C{=}C(HBR_2) \quad (1)$$

for Pd(0) and Pt(0), we can gain much insight into the experimentally observed differences between their catalytic behaviors. While the results for M = Pt have been published,[4] we have included some of them in the current paper to make easier comparison with M= Pd. In our previous studies,[2a,4] was shown that $(HO)_2B{-}B(OH)_2$ and $HB(OH)_2$ are good models for the pinacol ester and catechol borane, respectively. Therefore, we will continue using $(HO)_2B{-}B(OH)_2$ to model the pinacol ester derivatives used in the experiments. The $Pd(PR_3)_2$ complex is modeled by $Pd(PH_3)_2$.

II. Calculation Procedure and Evaluation of the Models

The geometries of the reactants, intermediates, transition states, and products of reaction 1 for M = Pd and R = OH are optimized using the B3LYP hybrid density functional theory[6] with a standard double-ζ quality basis set, lanl2dz, associated with the relativistic effective core potential (ECP) for the metals[7a] and the nonrelativistic ECP for phosphorus[7b] atoms (below denoted as BSI). Normal-mode analysis has been performed only for a few transition states, which will be described in more detail in the discussions. The energetics of the optimized structures were recalculated using a larger basis set (below denoted as BSII), which includes the double-ζ + polarization basis set of Dunning for the main group elements[8] and lanl2dz + polarization f function[9] for the transition-metal atoms. No zero-point correction was added to the energies presented in the tables. All calculations were performed by our modified Gaussian-92/DFT package.[10,11]

In our previous studies[4] we demonstrated that the current method is adequate to describe the geometries and relative energies of critical structures in reaction 1 for M = Pt. In the present studies we further tested the reliability of the B3LYP method for M = Pd. The calculated energy differences between the low-lying $^3D(s^1d^9)$ and $^1S(s^0d^{10})$ electronic states of the Pd and Pt atoms, as well as the $M{-}BR_2$, $M{-}PH_3$, and $PH_3{-}MPH_3$ binding energies of the MBR_2, MPH_3, and $M(PH_3)_2$ complexes (where M = Pd and Pt, and R = H and OH), at the B3LYP and CCSD(T) levels with the BSII are shown in Table 1. As seen in Table 1, the ground state of the Pd atom is calculated to be the $^1S(s^0d^{10})$ state. The high-spin state $^3D(s^1d^9)$ lies 14.5 and 19.2 kcal/mol higher at the CCSD(T) and B3LYP levels, respectively, versus 21.9 kcal/mol from the experiment.[12] However,

(1) (a) Brown, H. C. *Boranes in Organic Chemistry*; Cornell University Press: London, 1972. (b) Brown, H. C. *Organic Synthesis via Organoboranes*; Wiley-Interscience: New York, 1975. (c) Pelter, A.; Smith, K.; Brown, H. C. *Borane Reagents*; Academic Press: New York, 1988. (d) Manning, D.; Noth, H. *Angew. Chem., Int. Ed. Engl.* **1985**, *24*, 878. (e) Burgess, K.; Ohlmeyer, M. J. *Chem. Rev.* **1991**, *91*, 1179 and references therein. (f) Evans, D. A.; Fu, G. C.; Hoveyda, A. H. *J. Am. Chem. Soc.* **1988**, *110*, 6917. (g) Evans, D. A.; Fu, G. C. *J. Org. Chem.* **1990**, *55*, 2280. (h) Evans, D. A.; Fu, G. C. *J. Am. Chem. Soc.* **1991**, *113*, 4042. (i) Evans, D. A.; Fu, G. C.; Hoveyda, A. H. *J. Am. Chem. Soc.* **1992**, *114*, 6671. (j) Evans, D. A.; Fu G. C.; Anderson, B. A. *J. Am. Chem. Soc.* **1992**, *114*, 6679. (k) Burgess, K.; Cassidy, J.; Ohlmeyer, M. J. *J. Org. Chem.* **1991**, *56*, 1020. (l) Burgess, K.; Ohlmeyer, M. J. *J. Org. Chem.* **1991**, *56*, 1027. (m) Burgess, K.; Ohlmeyer, M. J. *Tetrahedron Lett.* **1989**, *30*, 395. (n) Burgess, K.; Ohlmeyer, M. J. *Tetrahedron Lett.* **1989**, *30*, 5857. (o) Burgess, K.; Ohlmeyer, M. J. *Tetrahedron Lett.* **1989**, *30*, 5861. (p) Burgess, K.; van der Donk, W. A.; Jarstfer, M. B.; Ohlmeyer, M. J. *J. Am. Chem. Soc.* **1991**, *113*, 6139. (q) Satoh, M.; Nomoto, Y.; Miyaura, N.; Suzuki, A. *Tetrahedron Lett.* **1989**, *30*, 3789. (r) Satoh, M.; Miyaura, N.; Suzuki, A. *Tetrahedron Lett.* **1990**, *31*, 231. (s) Brown, J. M.; Lloyd-Jones, G. C. *Tetrahedron: Asymmetry* **1990**, *1*, 869. (t) Hayashi, T.; Matsumoto, Y.; Ito, Y. *J. Am. Chem. Soc.* **1989**, *111*, 3426. (u) Hayashi, T.; Matsumoto, Y.; Ito, Y. *Tetrahedron: Asymmetry* **1991**, *2*, 601. (v) Matsumoto, Y.; Hayashi, T. *Tetrahedron Lett.* **1991**, *32*, 3387. (w) Burgess, K.; Ohlmeyer, M. J. *J. Org. Chem.* **1988**, *53*, 5178. (x) Burgess, K.; van der Donk, W. A.; Ohlmeyer, M. J. *Tetrahedron: Asymmetry* **1991**, *2*, 613. (y) Zhang, J.; Lou, B.; Guo, G.; Dai, L. *J. Org. Chem.* **1991**, *56*, 1670. (z) Westcott, S. A.; Blom, H. P.; Marder, T. B.; Baker, R. T. *J. Am. Chem. Soc.* **1992**, *114*, 8863. (aa) Westcott, S. A.; Taylor, N. J.; Marder, T. B.; Baker, R. T.; Jones, N. J.; Calabrese, J. C. *J. Chem. Soc., Chem. Commun.* **1991**, 304. (bb) Baker, R. T.; Ovenall, D. W.; Calabrese, J. C.; Westcott, S. A.; Taylor, N. J.; Williams, I. D.; Marder, T. B. *J. Am. Chem. Soc.* **1990**, *112*, 9399. (cc) Baker, R. T.; Ovenall, D. W.; Harlow, R. L.; Westcott, S. A.; Taylor, N. J.; Marder, T. B. *Organometallics* **1990**, *9*, 3028. (dd) Westcott, S. A.; Blom, H. P.; Marder, T. B.; Baker, R. T.; Calabrese, J. C. *Inorg. Chem.* **1993**, *32*, 2175. (ee) Harrison, K. N.; Marks, T. J. *J. Am. Chem. Soc.* **1992**, *114*, 9220. (ff) Burgess, K.; Jaspars, M. *Organometallics* **1993**, *12*, 497. (gg) Burgess, K.; Donk, W. A.; Kook, A. M. *J. Org. Chem.* **1991**, *56*, 2949. (hh) Knorr, J. R.; Merola, J. S. *Organometallics* **1990**, *9*, 3008. (ii) Burgess, K.; van der Donk, W. A.; Westcott, S. A.; Marder, T. B.; Baker, R. T.; Calabrese, J. C. *J. Am. Chem. Soc.* **1992**, *114*, 9350. (jj) Crabtree, R. H.; Davis, M. W. *J. Org. Chem.* **1986**, *51*, 2655. (kk) Westcott, S. A.; Marder, T. B.; Baker, R. T. *Organometallics* **1993**, *12*, 975. (ll) Baker, R. T.; Calabrese, J. C.; Westcott, S. A.; Nguyen, P.; Marder, T. B. *J. Am. Chem. Soc.* **1993**, *115*, 4367. (mm) Hartwing, J. F.; Bhandari, S.; Rablen, P. R. *J. Am. Chem. Soc.* **1994**, 116, 1839. (nn) Baker, R. T.; Nguyen, P.; Marder, T. B.; Westcott, S. A. *Angew. Chem., Int. Ed. Engl.* **1995**, *34*, 1336.

(2) (a) Musaev, D. G.; Mebel, A. M.; Morokuma, K. *J. Am. Chem. Soc.* **1994**, *116*, 10693. (b) Musaev, D. G.; Morokuma, K. *J. Phys. Chem.* **1996**, *100*, 6509. (c) Dorigo, A. E.; Schleyer, P. v. R. *Angew. Chem., Int. Ed. Engl.* **1995**, *34*, 878.

(3) (a) Ishiyama, T.; Nishijima, K.; Miyaura, N.; Suzuki, A. *J. Am. Chem. Soc.* **1993**, *115*, 7219 and references therein. (b) Ishiyama, T.; Matsuda, N.; Miyaura, N.; Suzuki, A. *J. Am. Chem. Soc.* **1993**, *115*, 11018. (c) Iverson, C. N.; Smith, M. R. A., III. *J. Am. Chem. Soc.* **1995**, *117*, 4403. (d) Suzuki, A. *Pure Appl. Chem.* **1994**, *66*, 213. (e) Gridnev, I. D.; Miyaura, N.; Suzuki, A. *Organometallics* **1993**, *12*, 589. (f) Lesley, G.; Nguyen, P.; Taylor, N. J.; Marder, T. B.; Scott, A. J.; Clegg, W.; Norman, N. C. *Organometallics* **1996**, *15*, 5137 and references therein.

(4) Cui, Q.; Musaev, D. G.; Morokuma, K. *Organometallics* **1997**, *16*, 1355.

(5) Cui, Q.; Musaev, D. G.; Morokuma, K. To be submitted for publication.

(6) (a) Becke, A. D. *Phys. Rev. A* **1988**, *38*, 3098. (b) Lee, C.; Yang, W.; Parr, R. G. *Phys. Rev. B* **1988**, *37*, 785. (c) Becke, A. D. *J. Chem. Phys.* **1993**, *98*, 5648.

(7) (a) Hay, P. J.; Wadt, W. R. *J. Chem. Phys.* **1985**, *82*, 299. (b) Wadt, W. R.; Hay, P. J. *J. Chem. Phys.* **1985**, *82*, 284.

(8) (a) Dunning, T. M., Jr. *J. Chem. Phys.* **1971**, *55*, 716. (b) Dunning, T. M., Jr. *J. Chem. Phys.* **1970**, *53*, 2823.

(9) Ehlers, A. W.; Böhme, M.; Dapprich, S.; Gobbi, A.; Höllwarth, A.; Jonas, V.; Köhler, K. F.; Stegmann, R.; Veldkamp, A.; Frenking, G. *Chem. Phys. Lett.* **1993**, *208*, 111.

(10) Frisch, M. J.; Trucks, G. W.; Head-Gordon, M.; Gill, P. M. W.; Wong, M. W.; Foresman, J. B.; Johnson, B. G.; Schlegel, H. B.; Robb, M. A.; Replogle, E. S.; Gomperts, R.; Andres, J. L.; Raghavachari, K.; Binkley, J. S.; Gonzales, C.; Martin, R. L.; Fox, D. J.; DeFrees, D. J.; Baker, J.; Stewart, J. J. P.; Pople, J. A. *GAUSSIAN 92/DFT*; Gaussian Inc.: Pittsburgh, PA, 1992.

(11) Cui, Q.; Musaev, D. G.; Svensson, M.; Morokuma, K. *J. Phys. Chem.* **1996**, *100*, 10936.

(12) Moore, C. F. *Atomic Energy Levels*; NSRDNBS; U.S. Government Printing Office; Washington, DC, 1971; Vol. III.

Scheme 1. Proposed Mechanism of the $M(PR_3)_2$-Catalyzed (M = Pd and Pt) Alkyne Diboration

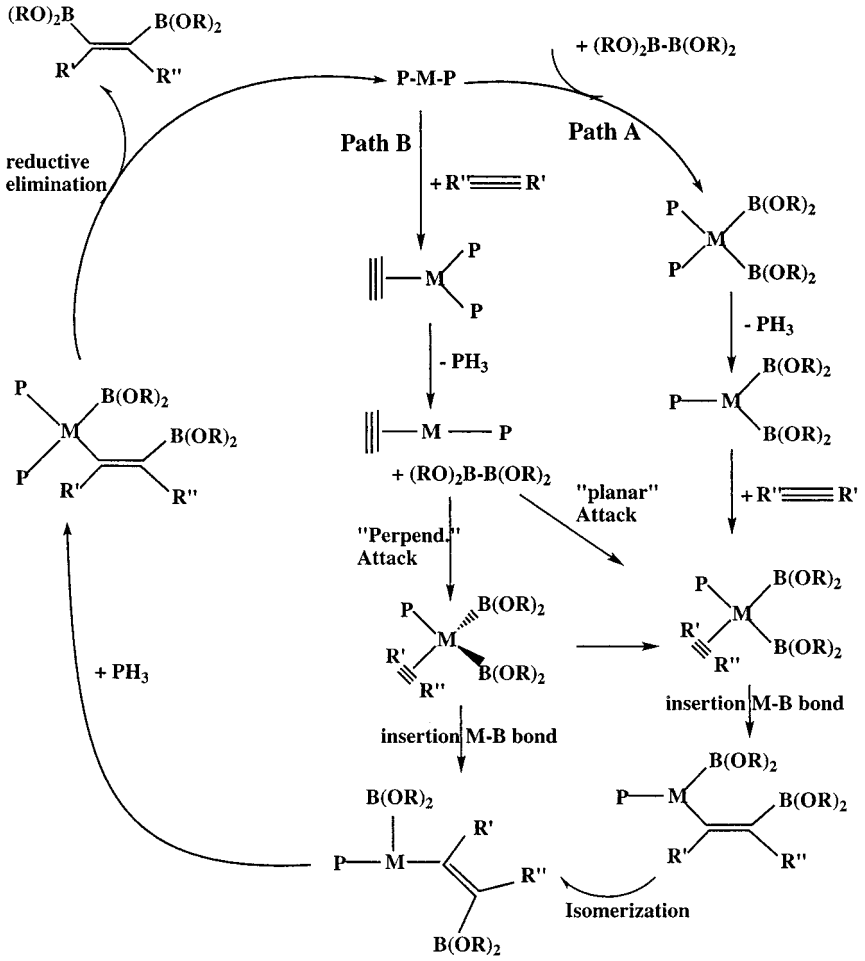

Table 1. Relative Energies (kcal/mol) of Two States of Atom M and the M−BR_2, M−PH_3, and PH_3−MPH_3 (M = Pd and Pt) Binding Energies (kcal/mol) at the B3LYP/II and CCSD(T)/II Levels Using the B3LYP/I Optimized Geometries[a]

	state	CCSD(T)/II	B3LYP/II	expt
Pd	^3D, s^1d^9	0.0	0.0	0.0
	^1S, s^0d^{10}	−14.6	−19.2	−21.9
Pt	^3D, s^1d^9	0.0	0.0	0.0
	^1S, s^0d^{10}	15.1	13.9	11.1
$PdBH_2$	$^2A_1$	62.0	66.8	
$PdB(OH)_2$	$^2A_1$	60.2	62.8	
$PtBH_2$	$^2A_1$	93.3	96.8	
$PtB(OH)_2$	$^2A_1$	91.0	89.1	
$PdPH_3$	$^1A'$	29.1	33.3	
$Pd(PH_3)_2$	$^1A_1$	28.7	27.3	
$PtPH_3$	$^1A'$	51.7	54.6 (56.6)[b]	
$Pt(PH_3)_2$	$^1A_1$	41.4	38.9 (38.3)[b]	

[a] The total energy of BR_2 is −25.817 789 and −25.935 421 au for R = H, and −176.066 975 and −176.547 552 au for R = OH at the CCSD(T)/II and B3LYP/II levels, respectively. The total energy of PH_3 is −8.210 04 and −8.30162 au at the CCSD(T)/II and B3LYP/II levels, respectively. No zero-point energy is included. [b] The numbers in parentheses are calculated using the B3LYP/II optimized geometries.

for the Pt atom the $^3D(s^1d^9)$ state is calculated[4] to be the ground state, and the $^1S(s^0d^{10})$ state is 15.1 and 13.9 kcal/mol higher at the CCSD(T) and B3LYP levels, respectively, versus 11.1 kcal/mol from the experiment.[12] Thus, the B3LYP/II approach gives better agreement with experiment than the CCSD(T)/II by a few kilocalories/mole, with only 2−3 kcal/mol off from the experimental values. As seen in Table 1, the M−BR_2, M−PH_3, and PH_3−MPH_3 binding energies of the MBR_2, MPH_3, and $M(PH_3)_2$ complexes, respectively, calculated at the CCSD(T) and B3LYP levels are different up to 4.0 kcal/mol regardless of the metal and substituents in the boryl group. Therefore, we conclude that the B3LYP/II//B3LYP/I approach used throughout the current paper is nearly as reliable as the CCSD(T)/II//B3LYP/I method.

Finally, we note that in the experiment $P(Ph)_3$ is used as a ligand, while we have used PH_3 in our calculations. We do not expect any qualitative change in the reaction mechanism because the Ph groups are planar and therefore do not cause as much steric repulsion as branched alkyl groups such as *tert*-butyl. However, the basicity of $P(Ph)_3$ and PH_3 might differ, and it might be interesting in the future to investigate the effect of this difference using our recently developed IMOMM, IMOMO, or ONIOM method.[13]

In section III, we briefly discuss the structures and bonding pictures of the reactants. In section IV we discuss the potential energy surface (PES) of reaction 1 for M = Pd. In section V we compare the PESs of reactions 1 between M = Pt and Pd. In the final section VI we make a few conclusions.

(13) (a) Svensson, M.; Humbel, S.; Froese, R. D. J.; Matsubara, T.; Sieber, S.; Morokuma, M. *J. Phys. Chem.* **1996**, *100*, 19357. (b) Matsubara, T.; Maseras, F.; Koga, N.; Morokuma, K. *J. Phys. Chem.* **1996**, *100*, 2573. (c) Humbel, S.; Sieber, S.; Morokuma, K. *J. Chem. Phys.* **1996**, *105*, 1959.

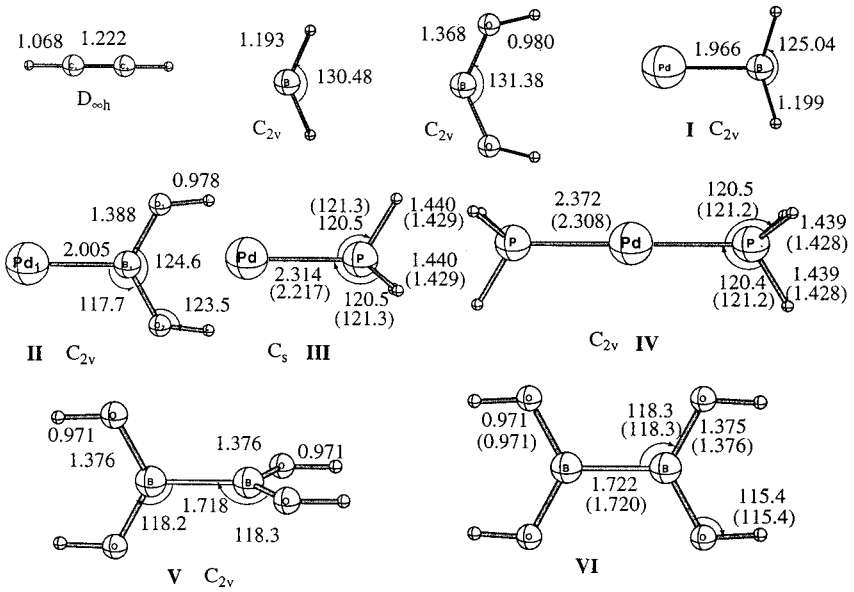

Figure 1. B3LYP/I optimized geometries (in Å and deg) of the $PdBR_2$ complex, BR_2 (where R = OH and H), and the reactants $PdPH_3$, $Pd(PH_3)_2$, and $[B(OH)_2]_2$. Numbers in parentheses are at the B3LYP/II level.

Table 2. Calculated MO Energies (au; B3LYP/I Level) and Mulliken Orbital Populations (B3LYP/II Level) for $M(PH_3)_2$ (Linear and Bent) and $(BR_2)_2M(PH_3)_2$ Where (M = Pd and Pt)

	M = Pd				M = Pt			
complex	irrep	eigenvalue	character	population	irrep	eigenvalue	character	population
linear $M(PH_3)_2$	a_1	−0.177 88	s/d_{z^2}	$s^{2.66}p^{6.05}d^{9.47}$	b_1	−0.193 41	d_{xz}	$s^{2.91}p^{5.98}d^{9.21}$
	a_1	−0.188 51	$d_{x^2-z^2}$		a_1	−0.193 45	$d_{x^2-z^2}$	
	b_1	−0.188 53	d_{xz}		a_1	−0.200 01	s/d_{z^2}	
	b_2	−0.214 37	d_{yz}		b_2	−0.235 30	d_{yz}	
	a_2	−0.214 37	d_{xy}		a_2	−0.235 32	d_{xy}	
	b_2	−0.294 96	M−PH_3		b_2	−0.306 82	M−PH_3	
	a_1	−0.364 13	M−PH_3		a_1	−0.412 65	M−PH_3	
bent[a] $M(PH_3)_2$	b_2	−0.158 66	d_{yz}	$s^{2.21}p^{6.22}d^{9.53}$	b_2	−0.161 33	d_{yz}	$s^{2.56}p^{6.19}d^{9.35}$
	a_1	−0.189 61	s/d_{z^2}		a_1	−0.196 94	s/d_{z^2}	
	b_1	−0.203 22	d_{xz}		b_1	−0.211 16	d_{xz}	
	a_2	−0.204 85	d_{xy}		a_2	−0.214 10	d_{xy}	
	a_1	−0.213 35	$d_{y^2-z^2}$		a_1	−0.228 03	$d_{y^2-z^2}$	
	b_2	−0.316 34	M−PH_3		b_2	−0.340 06	M−PH_3	
	a_1	−0.330 12	M−PH_3		a_1	−0.362 08	M−PH_3	
oxidative addition product	a_1	−0.195 06	M−B ant-b	$s^{2.66}p^{6.53}d^{9.09}$	a_1	−0.204 11	s/d_{z^2}	$s^{2.90}p^{6.49}d^{8.88}$
	a_1	−0.247 14	M−B bond		a_2	−0.243 95	d_{xy}	
	b_2	−0.249 77	M−B/PH_3		b_1	−0.245 18	d_{xz}	
	a_2	−0.251 11	d_{xy}		a_1	−0.248 35	M−B bond	
	b_1	−0.251 17	d_{xz}		b_2	−0.254 34	M−B/PH_3	
	a_1	−0.277 94	$d_{y^2-z^2}$		a_1	−0.279 23	$d_{y^2-z^2}$	

[a] At the $M(PH_3)_2$ geometry of the oxidative addition product $M(PH_3)_2[B(OH)_2]$.

III. Properties and Bonding Picture of the Reactants

The structures of the reactants of reaction 1, $Pd(PH_3)_2$, C_2H_2, and $B_2[(OH)_2]_2$, are shown in Figure 1. The Pd−P distance in $Pd(PH_3)_2$ is a little longer than the Pt−P distance in $Pt(PH_3)_2$. The bonding picture and stability of the complexes $Pd(PH_3)_2$ and $Pt(PH_3)_2$ were the subjects of extensive studies.[14] We will only briefly recall the main conclusions from previous studies[14] and compare them with our results. Of the two $B_2[(OH)_2]_2$ structures, we will use structure **VI**, as discussed previously.[4]

First of all it is well-documented[14] that the metal atom in the complex $M(PH_3)_2$ is Pd(0) or Pt(0) with the d^{10} configuration. Addition of two phosphines to M stabilizes d^{10} with respect to s^1d^9 so that the ground state of $M(PH_3)_2$ becomes a linear d^{10} singlet for both M = Pd and M = Pt. This stabilization of d^{10} arises from the donation of the phosphine lone pair to the empty metal s orbital (Lewis base/Lewis acid interaction), leading to strong bonding. The Mulliken populations of the metal atoms in the linear $M(PH_3)_2$ complexes in Table 2 are consistent with this conclusion.

Second, Goddard and co-workers[14b,c] concluded that the oxidative addition reaction A−B + $M(PH_3)_2$ → $(A)(B)M(PH_3)_2$ involves a change in the effective electronic configuration of M from a d^{10} configuration for $M(PH_3)_2$ to an s^1d^9 configuration for $(A)(B)M(PH_3)_2$. The reason is simple: the d^{10} configuration cannot make covalent bonds since all d^{10} orbitals are doubly occupied,

(14) (a) Obara, S.; Kitaura, K.; Morokuma, K. *J. Am. Chem. Soc.* **1984**, *106*, 7482. (b) Low, J. J.; Goddard, W. A., III. *J. Am. Chem. Soc.* **1986**, *108*, 6115. (c) Low, J. J.; Goddard, W. A., III. *Organometallics* **1986**, *5*, 609. (d) Hay, P. J. *Transition Metal Hydrides*; Dedieu, A., Ed.; VCH: Weinheim, 1992; pp 127−147 and references therein.

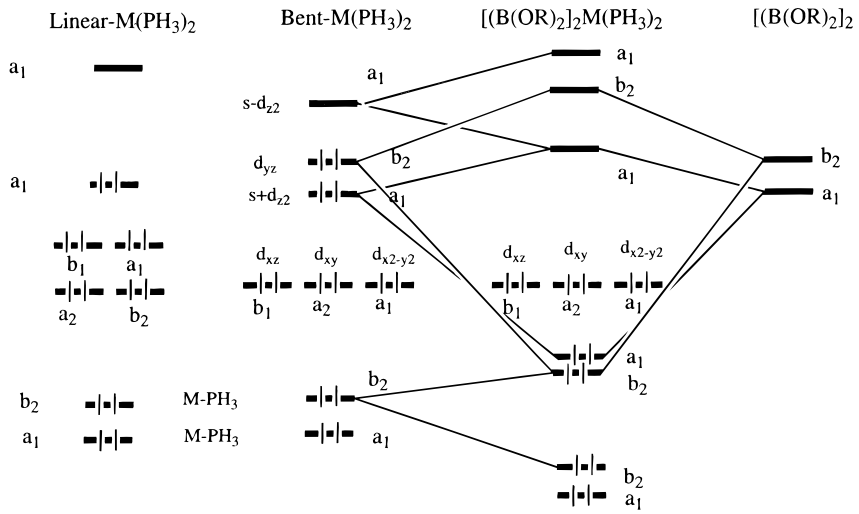

Figure 2. Orbital correlation diagram for $M(PH_3)_2[B(OR_2)]_2$, where M = Pd and Pt.

while the s^1d^9 configuration with two singly occupied orbitals can form two sd hybrids and is capable of forming covalent bonds. As has been pointed out, the oxidation state of Pd and Pt complexes should be interpreted in terms of maximum covalency rather than the degree of oxidation. In other words, the metal atom is not oxidized during the addition of the A−B σ bond, but rather the metal is promoted from the d^{10} state to the s^1d^9 state. The Mulliken population data presented in Table 2 for the $(BR_2)_2M(PH_3)_2$ complexes are consistent with this argument. On the other hand, during the reductive elimination reaction $(A)(B)M(PH_3)_2 \rightarrow A-B + M(PH_3)_2$ the electronic configuration of the M atom changes from s^1d^9 in $(A)(B)M(PH_3)_2$ to d^{10} in $M(PH_3)_2$.

According to the orbital correlation diagram in Figure 2 (see also Table 2), in the linear $M(PH_3)_2$ complex, d orbitals are split into three groups, two of which are degenerate. The highest occupied orbital (HOMO) is mainly the $s + d_{z^2}$ orbital of the metal atom. The low-lying unoccupied molecular orbitals (LUMOs) are M s $- d_{x^2}$ and p orbitals. Two M−PH_3 bonding orbitals lie below the d orbitals. Upon P−M−P bending, the arrangement of d orbitals changes from those in the linear structure; most significantly, the d_{yz} (b_2) orbital becomes the HOMO. The HOMO along with the LUMO (a_1, roughly $s - d_{z^2}$) will interact with the vacant $\sigma(b_2)$ and $\sigma(a_1)$ orbitals of the B−B group, leading to the oxidative addition of the B−B to the metal.

Finally, the calculated M−PH_3 and H_3PM-PH_3 binding energies of $M(PH_3)$ and $M(PH_3)_2$ are 33.3 and 27.3 kcal/mol for M = Pd and 54.6 and 38.9 kcal/mol for M= Pt, respectively, at the B3LYP/II level. The M−PH_3 and H_3PM-PH_3 bonds are 21.3 and 11.6 kcal/mol stronger for M = Pt than for M = Pd, respectively. Bearing the above discussion in mind, we can start our discussion on the mechanism of reaction 1 for M = Pd and Pt.

IV. The Mechanism of the Reaction $Pd(PH_3)_2 + C_2H_2 + R_2B-BR_2 \rightarrow Pd(PH_3)_2 + (HR_2B)C{=}C(HBR_2)$

As shown in Scheme 1, reaction 1 may proceed via two distinct paths, A and B. In path A the first step is coordination of R_2B-BR_2 to the Pd complex, while the first step of path B is coordination of acetylene to $Pd(PH_3)_2$. As mentioned in the Introduction, our previous papers on the Pt system[4,5] show that path A is the more favorable one when large substituted diborane and alkynes are used. Furthermore, we have shown[5] that, even for small diborane and alkynes, path B and path A actually merge at the square-planar $Pt(PH_3)(C_2H_2)(BR_2)_2$ complex. We expect a similar behavior in the current case for Pd. Therefore, we will investigate only path A in the present paper.

As mentioned above, the first step in path A is coordination of $(OH)_2B-B(OH)_2$ to $Pd(PH_3)_2$ which leads to the molecular complex $[(OH)_2B-B(OH)_2]Pd(PH_3)_2$ **VIII** with the B−B axis perpendicular to P−Pd−P, as shown in Figure 3. The geometries of the $(OH)_2B-B(OH)_2$ and $Pd(PH_3)_2$ fragments of complex **VIII** are very close to those in the free molecules, with the B−B distance 0.025 Å shorter, the Pd−P bond 0.033 Å longer, and the P−Pd−P angle 7.2° smaller. The Pd−B bond length of 2.605 Å clearly shows that the nature of the $[(OH)_2B-B(OH)_2]-Pd(PH_3)_2$ interaction is mostly a weak electron donation from the occupied metal d orbital to the empty p orbital of $(OH)_2B-B(OH)_2$, which is consistent with the rather small interaction energy of 3.5 kcal/mol. The molecular complex with the B−B axis parallel to P−Pd−P was found not to exist because of the unfavorable steric repulsion.

From **VIII** the reaction proceeds via activation of the B−B bond throughout transition state **IX**. As seen in Figure 3, the B−B, Pd−B, and Pd−P bonds in **IX** are about 0.24 Å longer, 0.44 Å shorter, and 0.075 Å longer, respectively, than those in complex **VIII**. The P−Pd−P angle is reduced from 172.8° to 106.5°. These results, as well as the normal-mode analysis with one imaginary frequency of 123.6i cm^{-1}, clearly show that **IX** is a real transition state for B−B bond activation. The activation barrier is calculated to be 8.6 kcal/mol relative to complex **VIII**. The oxidative addition product **X** with the well-known square-planar structure is only about 0.1 kcal/mol lower than the activation barrier **IX**. In **X** the OBO planes are perpendicular to each other to avoid steric repulsion. A set of Pd−P bond lengths often differ by a few hundredths of angstrom, and an average value will be used in the discussions. As seen in Figure 3,

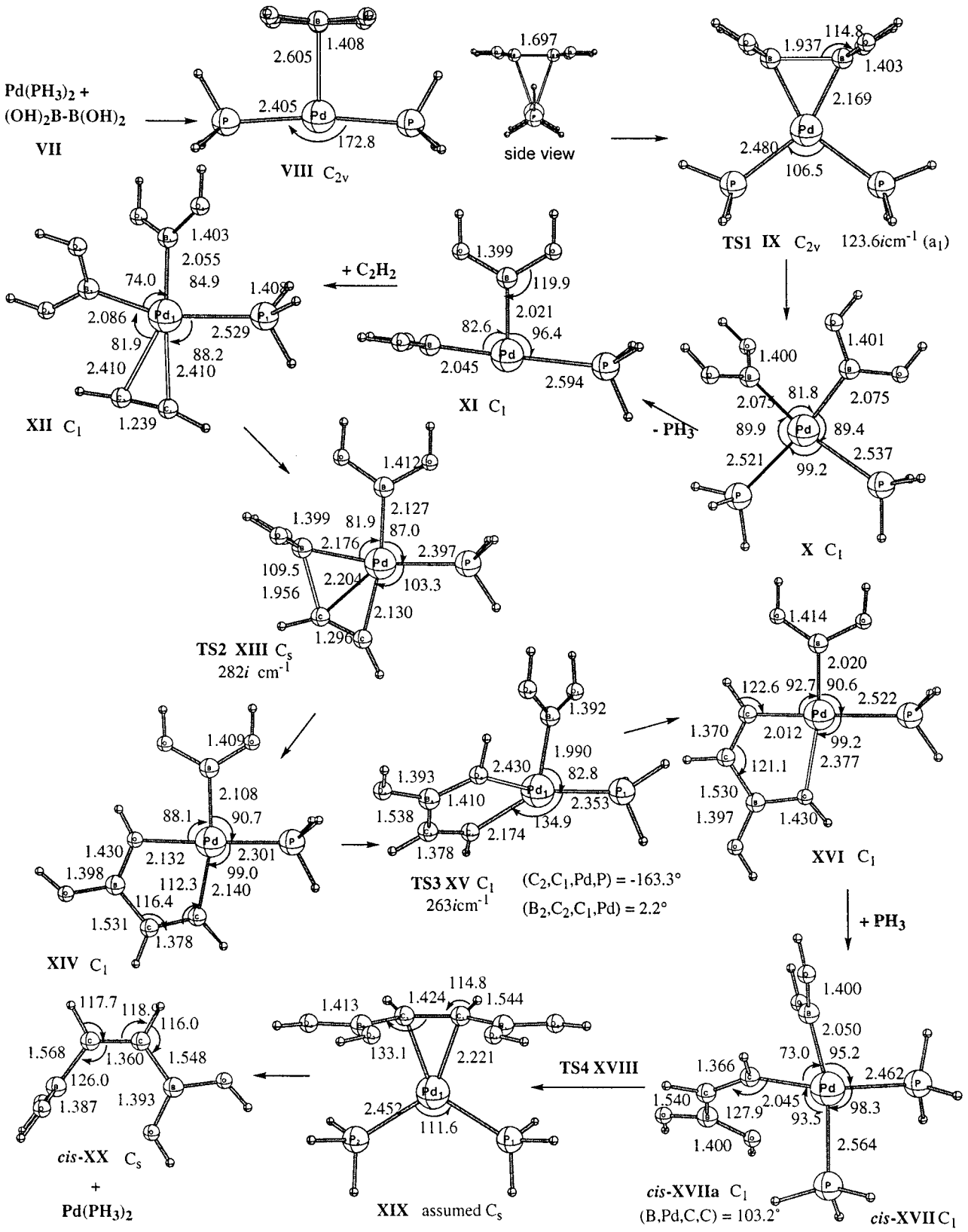

Figure 3. B3LYP/I optimized geometries (in Å and deg) of the intermediates and transition states of reaction 1 for M = Pd.

the Pd−P bond in **X** is significantly stretched, from 2.37 Å in free $Pd(PH_3)_2$ to 2.53 Å. As mentioned in our previous paper,[4] the metal−P bond distance is rather sensitive to the quality of the basis set on P; the polarization function can shorten the Pt−P distance as much as 0.1 Å, while it does not change significantly either other geometrical parameters or the relative energies. We may expect similar effects in the case of Pd.

From **X** the reaction may proceed in two possible ways, either (1) by coordination of the incoming acetylene and formation of the five-coordinate complex

$[(OH)_2B]_2Pd(PH_3)_2(C_2H_2)$ or (2) via dissociation of one of the phosphine ligands to form the three-coordinate complex $[(OH)_2B]_2Pd(PH_3)$ followed by coordination of acetylene. No five-coordinate complex $[(OH)_2B]_2Pd(PH_3)_2(C_2H_2)$ was actually found. Similar results have been found in a previous study on $Pd(PH_3)_2$-catalyzed silastannation of acetylene.[15] Therefore, at first, dissociation of a PH_3 ligand has to take place from **X**, which leads to the three-coordinate unsaturated complex **XI** with a well-defined T-shaped structure. This conclusion also is consistent with recent experimental finding; Iverson and Smith found that the stoichiometric results exclude simple, bimolecular insertion of an alkyne into Pt−B bonds of $(Ph_3P)_2Pt(Bcat)_2$ and that the observed dependence on phosphine and alkyne strongly favors a mechanism where phosphine dissociation generates a three-coordinate intermediate that mediates alkyne insertion.[16] The calculated Pd−B bond distances are shortened in **XI**, relative to those in **X**, by 0.030 and 0.054 Å for B *cis* and *trans* to the open site, respectively. The PH_3 dissociation energy is calculated to be 18.8 kcal/mol. Following the dissociation of PH_3, acetylene coordinates to **XI** at the open site to form structure **XII**. This structure is rather floppy; the C_2H_2 group may rotate nearly freely around the Pd−*X* axis, X being the center of the C−C bond of C_2H_2, with a barrier of less than 1 kcal/mol. Structure **XII** shown in Figure 3 is optimized with the constraint that C−C−Pd−P is coplanar. Since the Pd−C distance is rather long, 2.410 Å, and the C−C bond is very close to that in the free molecule C_2H_2, one may consider structure **XII** as a π complex. Forcing the C−C part to be perpendicular to the P−Pd−B plane results in a structure with nearly the same energy. The coordination energy of C_2H_2 to **XI** is calculated to be 12.3 kcal/mol. Thus, overall **XII** lies 11.5 kcal/mol *higher* than the reactants.

The next step of the reaction is the insertion of C_2H_2 into the Pd−B bond to form an intermediate **XIV**. During this process one of the Pd−B bonds and one of the C−C π bonds are broken, and one Pd−C σ bond is formed. The $B(OH)_2$ group rotates around the newly formed B−C bond so that the oxygen atom can interact with the open site of Pd. Consequently, the length of this interacting O−B bond is stretched to 1.430 Å, compared with the 1.398 Å of the O−B bond pointing away from the metal. The calculated Pd−P bond is shortened from 2.529 Å in **XII** to 2.301 Å in **XIV**, obviously due to the loss of a strong trans influence. The stage is calculated to be exothermic by 27.2 kcal/mol.

The transition state for insertion, **XIII**, has C_s symmetry. Normal-mode analysis shows that the structure has one imaginary frequency of 282i cm^{-1} in an a′ irrep (irreducible representation). Note that the lowest frequency is calculated to be 19 cm^{-1} in a″ irrep, corresponding to rotation of a $B(OH)_2$ ligand around the B−C bond. C_2H_2 is much closer (by 0.07 Å) to the metal in **XIII** than in **XII**. The C−C bond is stretched by 0.06 Å, and the $H^1-C^1-C^2$ and $H^2-C^2-C^1$ angles are decreased from 165.8° to 137.8° and 142.7°, respectively, clearly showing the change of hybridization of the carbon atoms to sp^2. The breaking Pd−B bond is 0.090 Å longer than in **XII**. The barrier height from **XII** is calculated to be 5.7 kcal/mol.

As discussed in the case of the Pt(0)-catalyzed diboration reaction,[4] the next step is the migration of the CH═CH[$B(OH)_2$] ligand, from being trans to the $B(OH)_2$ ligand in complex **XIV** to being cis in the complex **XVI**. This process from **XIV** to **XVI** is exothermic by 16.9 kcal/mol. The reason why **XVI** is more stable than **XIV** is the arrangement of strong donating ligands; the two strong ligands $B(OH)_2$ and CH═CH[$B(OH)_2$] are trans to each other in **XIV** and cis to each other in **XVI**. Thus the Pd−B and Pd−C bonds are weaker in **XIV** than in **XVI**, as seen from the bond distances. For example, the Pd−C bond is 0.13 Å longer in **XIV** than in **XVI**.

The optimized migration transition state **XV** has a Y shape, as shown in Figure 3. Normal-mode analysis confirms that this structure has one imaginary frequency of 263i cm^{-1}. The CH═CH[$B(OH)_2$] group also rotates around the Pd−C bond to avoid repulsion with the $B(OH)_2$ ligand and to retain the energy of coordination to the metal at the O end, with the B−C═C−Pd and C═C−Pd−P dihedral angles of 2.2° and −163.3° at TS3 **XV**. As the CH═CH[$B(OH)_2$] ligand moves from the trans to the cis position (relative to the $B(OH)_2$ ligand), the B−Pd−P angle of 90.7° in **XIV** decreases to 82.8° at the TS3 **XV** and then increases back to 90.6° in the product **XVI**. The isomerization barrier height is calculated to be 15.0 kcal/mol relative to **XIV**.

As seen in Figure 3, one of the O−H bonds of the CH═CH[$B(OH)_2$] group in TS **XV** is twisted with the $H-O^4-B^2-O^2$ dihedral angle of ∼40° instead of the ∼0.0° angle in all other structures. However, this twist cannot take place in the real cyclic diborane and must be an artifact of the model $B(OH)_2$. In order to examine the effect of possible twist in the real system, we have performed additional calculations for the structures **XIV′**, **XV′**, and **XVI′** with a more realistic model system $(OH)_2B-B(OCH_2)_2$ at the same level of the theory. The calculated geometries are presented in Figure 4, while the relative energies are given in Table 3, for both M = Pd and M = Pt. Clearly, geometrical parameters critical for the reaction in these structures hardly change. Furthermore, as seen from Table 3, the relative energies of **XV**, **XVI**, and **XVII** are very similar for the two models $B_2[(OH)_2]_2$ and $(OH)_2B-B(OCH_2)_2$. Therefore, we conclude that the twist in $B(OH)_2$ is not of serious concern.

In the next step recoordination of PH_3 to **XVI** takes place without barrier and leads to the complex **XVII**. The complex **XVII** has a square-planar structure, where the Pd−P bond trans to $B(OH)_2$, 2.564 Å, is longer than that trans to $CH=CHB(OH)_2$, 2.462 Å, reflecting the weaker trans influence of the latter as was discussed for **XIV** and **XVI** above. The B−Pd−C═C dihedral angle is 103.2°, indicating that the $CB(OH)_2$ group is out of plane from the nearly square coplanar P−PdB−C backbone and lost the O···Pd interaction. In principle, complex **XVII** may have another isomer where the $B(OH)_2$ group is trans with respect to the C═C bond. As shown in the previous paper,[4] this structure is actually a few kilocalories/mole more stable than the cis structure for M = Pt. However, the isomerization from the trans to the cis is not likely to take place

(15) Hada, M.; Tanaka, Y.; Ito, M.; Murakami, M.; Amii, H.; Ito, Y.; Nakatsuji, H. *J. Am. Chem. Soc.* **1994**, *116*, 8754.

(16) Iverson, C. N.; Smith, M. R., III. *Organometallics* **1996**, *15*, 5155.

(17) Yamamoto, A. *Organotransition Metal Chemistry*; John-Wiley & Sons: New York, 1986.

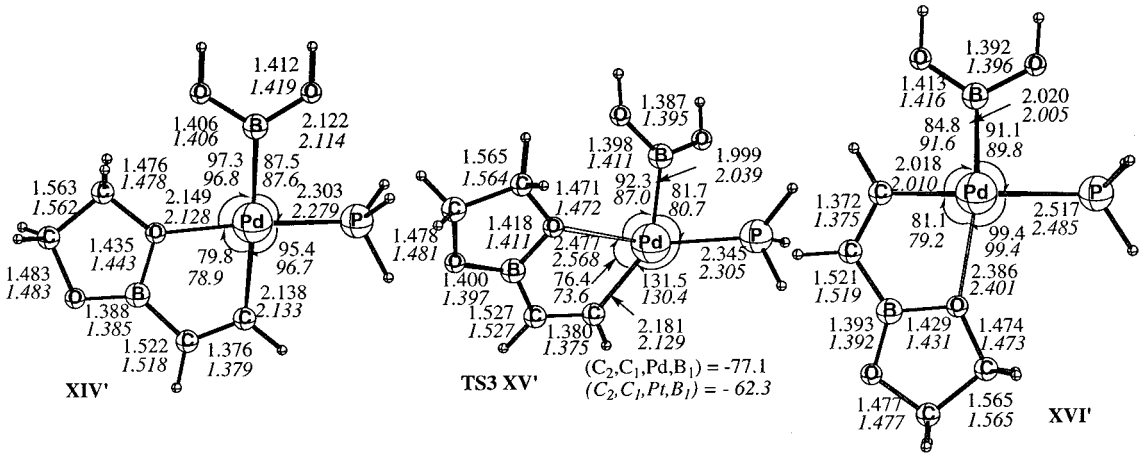

Figure 4. B3LYP/I optimized geometries (in Å and deg) of *trans*- and *cis*-$[B(OH)_2]M(PH_3)(CHCH[B(OCH_2)_2])$ (**XIV′** and **XVI′**, respectively), and the connecting transition state **XV′**, where M = Pd and Pt (in italics).

Table 3. Total Energy (au; Italics) of Reference Systems and Relative Energies (kcal/mol) Relative to $M(PH_3)_2 + [B(OH)_2]_2 + C_2H_2$ (M = Pd and Pt) of Intermediates and Transition States Involved in Path A of the Diboration Reaction at the B3LYP/II Level at the B3LYP/I Optimized Geometries[a]

compd	Pd	Pt
$M(PH_3)_2$, **IV**	*−143.40649*	*−135.8314*
$B_2(O_2H_2)_2$, **VI**	*−353.2644*	*−353.2644*
C_2H_2	*−77.3307*	*−77.3307*
PH_3	*−8.3016*	*−8.3016*
VIII	−3.5	−3.7
TS1, **IX**	5.1	10.3
X	5.0	−10.9
XI	23.8	7.9
XII	11.5	−5.0
TS2, **XIII**	17.2	4.0
XIV	−15.7 (−16.4/−16.3)[b]	−33.1 (−14.0/−13.9)
TS3, **XV**	0.7 (0.0/0.0)	−19.1 (0.0/0.0)
XVI	−32.6 (−33.3/−34.1)	−50.3 (−31.2/−34.6)
XVII	−38.2	−54.4
TS4, **XVIII**		−42.0
XIX	−73.5	−73.2
products, **XX**	−60.8	−60.8

[a] No zero-point energy is included. [b] The numbers in the parentheses are calculated relative to the isomerization transition state **XV**. The numbers before the slash stand for reaction 1 with $B_2[(OH)_2]_2$, while the numbers after the slash stand for reaction 1 with $(OH)_2B-B(OCH_2)_2$ (see the text for more detail).

because of a high barrier. The binding energy of PH_3 from **XVI** to **XVII** is 5.6 kcal/mol, as the interaction between Pd and O is lost in **XVII**. However, it should be noted that recoordination of this second PH_3 ligand is definitely needed to stabilize the following reductive elimination process, to avoid a highly unsaturated intermediate. The combined process from **XIV** to **XVII** is 22.5 kcal/mol exothermic.

From **XVII** the reductive elimination of the *cis*-$B(OH)_2CH{=}CHB(OH)_2$ product takes place. Although a transition state has been found and characterized for M = Pt,[4] for M = Pd we were unable to locate a transition state **XVIII**. All our attempts led either to the product **XIX** or back to **XVII**. Since the overall process **XVII** → **XX** is highly exothermic (by 22.5 kcal/mol), one expects this transition state to be very early and the barrier to be extremely small. The product complex **XIX** is a typical π complex, with a Pd−C distance of 2.221 Å. The binding energy of **XIX** relative to the final products *cis*-$B(OH)_2CH{=}CHB(OH)_2$ and Pt-$(PH_3)_2$ is 12.7 kcal/mol. The entire reaction 1, which is nothing but the reaction of C_2H_2 and $[B(OH)_2]_2$ to form *cis*-$B(OH)_2CH{=}CHB(OH)_2$, is exothermic by 60.8 kcal/mol.

V. Comparison of the Mechanisms of Pd(0)- and Pt(0)−Catalyzed Alkyne Diboration Reactions

In this section we will compare the PESs of alkyne diboration reaction 1 for M = Pt(0), reporteed in our previous paper,[4] and M = Pd(0) in the present paper. The energetics of the intermediates and transition states involved in reaction 1 for M = Pt is listed along with that for M = Pd in Table 3. The same labels are used for the corresponding structures for M = Pd and M = Pt. Schematic potential energy surfaces for both metals are shown in Figure 5.

For convenience of discussion, we can divide the entire PESs of reaction 1 for M = Pd and Pt into several stages, as shown in Figure 5. Stage a includes the reactants **VII** and the formation of the molecular complex $[(OH)_2B-B(OH)_2]M(PH_3)_2$, **VIII**; stage b covers the processes from **VIII** to **X** that is, **VIII** → **IX** → **X**; stage c starts from the oxidative addition product **X** and covers the processes **X** → **XI** → **XII** → **XIII** → **XIV** → **XV** → **XVI** → **XVII** leading to the inserted product $[CHCHB(OH)_2]M(PH_3)_2B(OH)_2$, **XVII**. The last stage (d) covers the processes **XVII** → **XVIII** → **XIX**. As seen in Table 3 and Figure 5, the PESs are quite similar for M = Pd(0) and Pt(0) on a relative scale for stages a and c. The calculated complexation energies, **VII** → **VIII**, are similar: 3.5 and 3.7 kcal/mol for M = Pd and Pt, respectively. The dissociation energy of PH_3 (the process **X** → **XI**), the coordination energy of C_2H_2 (**XI** → **XII**), the insertion barrier height (**XII** to **XIII**), and the isomerization barrier height (**XIV** → **XV**) are also similar: 18.8 (18.8), 12.3 (12.9), 6.3 (9.0), and 16.4 (14.0) kcal/mol for M = Pd and Pt (in parentheses), respectively. The processes from **XII** to **XIV**, from **XIV** to **XVI**, and from **XVI** to **XVII** are exothermic by 27.2 (28.1), 16.9 (17.2), and 5.6 (4.1) kcal/mol for M = Pd and Pt (in parentheses), respectively.

However, the processes in stages b (**VIII** → **IX** → **X**) and d (**XVII** → **XVIII** → **XIX**) have several clear differences between Pd and Pt systems. First of all, the oxidative addition reaction $R_2B-BR_2 + M(PH_3)_2$ →

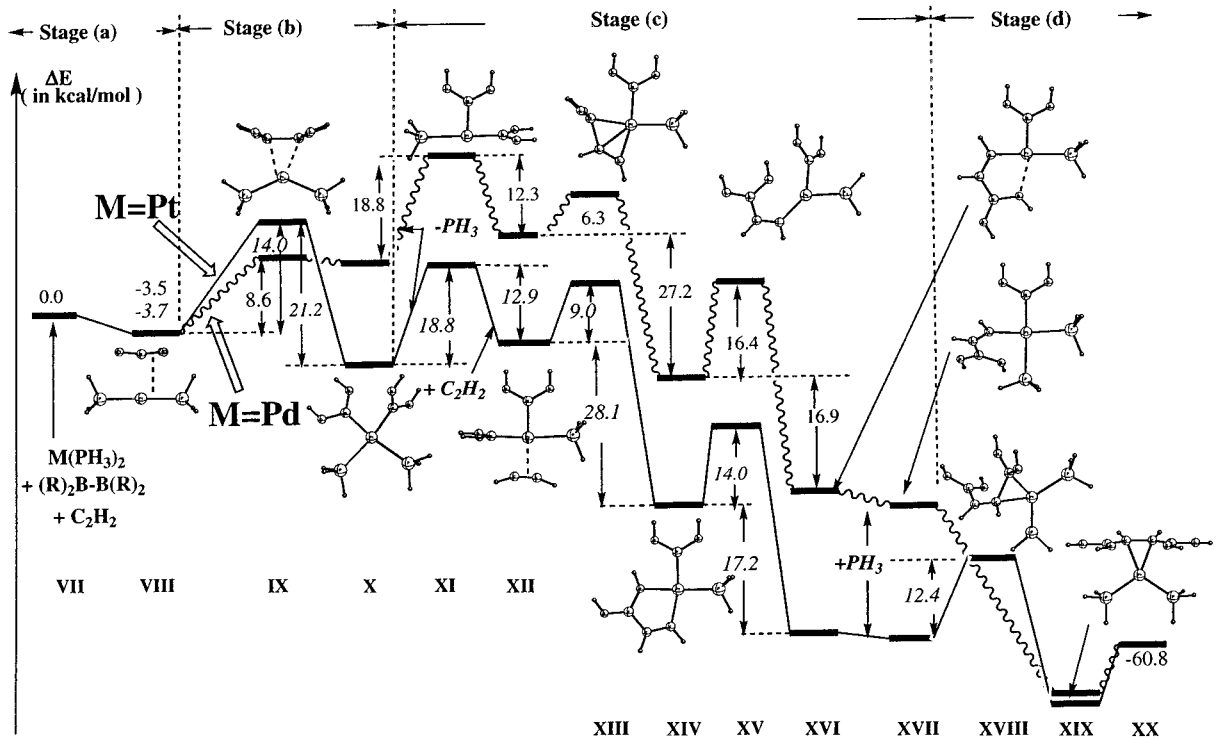

Figure 5. Comparison of the potential energy profiles for path A of the reaction: $M(PH_3)_2 + C_2H_2 + (OH)_2B-B(OH)_2 \rightarrow M(PH_3)_2 + C_2H_2[B(OH)_2]_2$, where M = Pd (wavy lines and roman type) and Pt (straight lines and italic type).

$(BR_2)_2M(PH_3)_2$ is 5.0 kcal/mol *endothermic* for M = Pd, while it is 10.9 kcal/mol *exothermic* for M = Pt, measured from the reactants. This difference in the stability of the B−B oxidative addition product of $Pd(PH_3)_2$ and $Pt(PH_3)_2$ can be understood by recalling the discussion on the electronic structures of $M(PH_3)_2$ and $(BR_2)_2M(PH_3)_2$ in section III. In the reaction the Pd and Pt atoms are promoted from the d^{10} configuration in $M(PH_3)_2$ to the s^1d^9 configuration, which is capable of forming two covalent bonds. Since the energy gap, that is, the promotion energy from the d^{10} to the s^1d^9 configuration, is much larger for Pd, the oxidative addition product $(BR_2)_2M(PH_3)_2$ is much less stable for M = Pd than for M = Pt.

The calculated oxidative addition barrier at the transition state **IX** from the molecular complex **VIII** is 8.6 and 14.0 kcal/mol for M = Pd and Pt, respectively. This seems to be contradictory to the fact that Pd−B bonds are weaker than Pt−B bonds. However, comparison of the structures of the transition state **IX** in Figure 3 shows that, although most geometrical parameters are very similar for Pd and Pt, the P−M−P angle is very different: 106.5° for Pd and 139.5° for Pt. As discussed in section III, with the smaller P−M−P angle, the d_{yz} orbital in Pd is further raised in energy and can interact more efficiently with the σ^* orbital of B−B. In addition, it is found that the P−M−P bending requires less energy for Pd than for Pt; bending from ∠PMP = 180° to 140° for $Pd(PH_3)_2$ needs only half as much energy (6.1 kcal/mol) as for $Pt(PH_3)_2$ (12.0 kcal/mol). Overall, the activation energy is smaller for Pd than Pt. A similar conclusion has been made by Sakaki et al. on the study of the oxidative addition of the Si−X σ bond to the $M(PH_3)_2$ complex (where M = Pd and Pt).[18]

(18) Sakaki, S.; Ogawa, M.; Musashi, Y, Arai, T. *Inorg. Chem.* **1994**, *33*, 1660.

Because of the low TS and the high endothermicity, the oxidative addition product **X** for Pd is only 0.1 kcal/mol lower than the transition state **IX**, in contrast to Pt, where it is 21.2 kcal/mol lower. The oxidative addition product for Pd is likely to eliminate the diborane easily to go back to the reactant complex, before the next step of reaction can take place. Despite a slightly higher barrier, the next step can take place for Pt due to the thermodynamic driving force, that is, the higher reverse barrier.

To summarize, $Pd(PH_3)_2$ does not catalyze the diboration reaction because the initial step of oxidative addition is not a favorable process, whereas its Pt analogue does activate the B−B bond and effectively catalyzes the reaction.

Finally, another difference is noticed in stage d. As seen in Figure 5, the elimination process **XVII** → **XX** for M = Pt is exothermic by 6.4 kcal/mol and takes place with a 12.4 kcal/mol elimination barrier at the transition state **XVIII**. However, it is highly exothermic (by 22.6 kcal/mol) for Pd and takes place without a barrier. This difference can be explained by recalling that, during this process, the electronic configuration of the M atom changes from s^1d^9 in $[B(OH)_2CHCH]M[B(OH)_2](PH_3)_2$ to d^{10} in $M(PH_3)_2$. Therefore, this reductive elimination reaction is more exothermic for Pd where d^{10} is the ground state than for Pt, which has the s^1d^9 ground state with d^{10} lying 13.9 kcal/mol higher.

VI. Conclusions

From the current study we may draw the following conclusions:

(1) The Pd(0)-catalyzed acetylene diboration reaction (path A) should proceed via the same mechanism as in the Pt(0)-catalyzed reaction and involves (i) coordination

of the R_2B-BR_2 molecule to the Pd(0) complex, (ii) oxidative addition of the B−B bond to the Pd(0) complex, (iii) dissociation of one phosphine ligand, (iv) coordination of acetylene to the Pd atom, (v) insertion of acetylene into a Pd−B bond, (vi) isomerization of the resultant complex, accompanied by recoordination of a phosphine ligand, and (vii) reductive elimination of the alkenyl−diboron product.

(2) However, the Pd(0) complex cannot catalyze alkyne diboration reaction 1, while its Pt(0) analogue can. The main origin for this difference in the catalytic activities beween Pd(0) and Pt(0) exists in the oxidative addition process of the B−B bond to $M(PH_3)_2$. The process occurs for M = Pt with a 14.0 kcal/mol activation barrier and is exothermic by 7.2 kcal/mol. Although the process for M = Pd has a lower (8.6 kcal/mol) barrier, it is 8.5 kcal/mol endothermic, and the reverse barrier is only 0.1 kcal/mol! Because of this low reverse barrier, B−B oxidative addition to $Pd(PH_3)_2$ cannot take place. The reason behind this difference has been explained in terms of the promotion energy from the d^{10} to the s^1d^9 configuration of the M(0) metal atoms, which is much larger for Pd than Pt.

Acknowledgment. The authors express their gratitude to Prof. T. B. Marder for very useful and intensive discussions of these and related results. The use of computational facilities and programs at the Emerson Center is acknowledged. The present research is in part supported by a grant (CHE-9627775) from the National Science Foundation. A Phillips Petroleum Co. graduate fellowship to Q.C. is acknowledged.

OM970277G